



HAL
open science

Semi-analytical model development for preliminary study of 3D woven Composite/Metallic flange bolted assemblies

Wafaa El Masnaoui, Alain Daidié, Frederic Lachaud, Christian Paleczny

► **To cite this version:**

Wafaa El Masnaoui, Alain Daidié, Frederic Lachaud, Christian Paleczny. Semi-analytical model development for preliminary study of 3D woven Composite/Metallic flange bolted assemblies. *Composite Structures*, 2021, 255, pp.112906. 10.1016/j.compstruct.2020.112906 . hal-03005577

HAL Id: hal-03005577

<https://hal.science/hal-03005577>

Submitted on 21 Sep 2022

HAL is a multi-disciplinary open access archive for the deposit and dissemination of scientific research documents, whether they are published or not. The documents may come from teaching and research institutions in France or abroad, or from public or private research centers.

L'archive ouverte pluridisciplinaire **HAL**, est destinée au dépôt et à la diffusion de documents scientifiques de niveau recherche, publiés ou non, émanant des établissements d'enseignement et de recherche français ou étrangers, des laboratoires publics ou privés.



Distributed under a Creative Commons Attribution - NonCommercial 4.0 International License

Semi-Analytical Model Development for Preliminary Study of 3D Woven Composite/Metallic Flange Bolted Assemblies

Wafaa EL MASNAOUI^{a,b}, Alain DAIDIE^{a,1}, Frédéric LACHAUD^a,
Christian PALECZNY^b,

^a*Institut Clément Ader, 3 Rue Caroline Aigle, 31400 Toulouse*

^b*Safran Aircraft Engines, Rond-point René Ravaut, 77550 Moissy Cramayel*

Abstract

This research deals with the development of a new semi-analytical model for composite-metal eccentric tensile bolted joints of casing structures. The model is based on a direct stiffness method considering structural elements, where flanges are modeled with axisymmetric shell elements, the bolt with a beam element and contact behavior with a specific number of compressive linear springs, identified by means of convergence tests. A hybrid element is added in order to set the link between flange and bolt. Since the model is intended for the preliminary design of bolted joints including composite materials, we propose an extension of the stiffness matrix formulation of isotropic axisymmetric shell elements to orthotropic ones. This formulation is validated with respect to a 2D FE axisymmetric model. Then, a semi-

¹ Corresponding author

Email address: alain.daidie@insa-toulouse.fr (Alain DAIDIE)

analytical model is established for a casing assembly approximately corresponding to a real casing of an aircraft engine. Design criteria such as normal stress on the bolt, bending moment and axial load at a specific section of the composite flange, given by the semi-analytical model are compared to a 3D FE computation. Results are in very good agreement and the semi-analytical model offers considerable time saving where the computation time was 120 times faster than the 3D FE model. Moreover, relative error does not exceed 2% for normal stress of the bolt and 9% for the flange bending moment which is satisfactory in a preliminary design approach. However, due to the formulation of hybrid element, less accurate results were observed for axial displacement of the composite flange and it would be advisable to consider a new formulation. This will be detailed in future work. Finally, a parametric study showed the ability of the semi-analytical model to predict the physical behavior of joints and proved its usability for running optimization studies and its reliability as a preliminary design tool.

Keywords: Bolted joints, 3D Woven composite, Orthotropic behavior, Direct Stiffness Method, Semi-analytic, Parametric study

1. Introduction

Composite materials are increasingly being used in many engineering applications because of their high strength to weight ratio. One of the major applications of composite materials is in aerospace structures where the weight reduction is a challenging issue. For example, the landing gear brace for the Boeing 787-8 Dreamliner and the fan blades and casings in the CFM LEAP engine all utilize composite materials reinforced with 3D woven carbon

fiber. Three-dimensional composite materials offer many advantages compared to two-dimensional reinforcement and laminate composites, such as improved fracture toughness and impact resistance, and stronger through-the-thickness behavior, while still carrying in in-plane loads [1–3].

Due to the facility with which they can be assembled and repaired, fasteners and bolts provide the most commonly used method of assembling composite structures, especially when metals are to be joined to composite materials. However, fastener and composite bolted joints should be carefully designed because of the sensitivity of composite around the hole. Thus, the study of bolted joints is necessary and has been the subject of many research works. First, the complex behavior of this joint was investigated by means of experimental studies. Warren et al. [4] investigated the bearing behavior of three architectures: 3D orthogonal, ply to ply 12K/24K and ply to ply 24K/24K, and concluded that bearing stiffness underwent a reduction in offaxis performance ranging from 24.7% to 32.7% and that materials with threedimensional reinforcement showed non-catastrophic bearing failures due to matrix cracking and tow distortion. More experiments were conducted by McCarthy et al. in [5] on laminate composites, to study the effect of bolthole clearance in a single-lap, single-bolt joint and extend it to single-lap, multi-bolt composite joints in [6]. Clearance was found to have no significant effects on the ultimate quasi-static strength of the joint but had an effect on load distribution and failure mode. Other experiment studies have investigated the pull through failure mode in composite joints [7, 8].

Bolted joint strength depends on many parameters, and controlling these parameters by means of experimental studies could be expensive. Thus, several authors have proposed numerical models in order to explain

mechanical behavior of composite bolted joints. Kyle et al. completed the experimental work detailed in [4] with an FE model by including damage behavior represented with a voxelized meso-scale model around the hole and an orthotropic material far from the bearing area [9]. Results were in good agreement with experimental data and the model also predicted progressive damage failure well. Camanho and Mathews applied quite a similar approach to composite laminates in [10]. Without accounting for damage behavior, McCarthy et al. developed a three dimensional FE model of a single-bolt, single-lap composite joint in [11]. These authors noted the importance of contact definition and showed the difficulties of modeling contact between the joint parts, which affected the accuracy and efficiency of the model. In fact, contact behavior can be difficult to control and depends on the contact and friction modeling used in the study. McCarthy et al. [12] performed Finite Element Analysis on single-lap bolted joint by comparing two friction models: the continuous friction model and the stick-slip model. A conclusion of this study was that both models are able to predict the load-deflection curve but the accuracy of the continuous model can be affected by a velocity parameter that results in signs of instability.

Numerical and Finite Element Analysis usually provide good results and are not as expensive as experiments, although they are still highly time consuming. However, the efficiency of this type of analysis can be improved by using simplified FE approaches that could also be employed as optimization and design tools. For example, Ekh and Schon [13] used beam elements to model the bolts and laminates, and connector elements for bolt-hole clearance and friction effect. Gray and McCarthy[14] adopted a similar approach and developed a user-defined element accounting for physical

interactions between the hole and the bolt, the user-defined element being combined with a shell element modeling laminates. The main advantages of this type of models is that they can be combined with analytical models in order to better capture some physical behavior, such as bolt extension and stiffness of the clamped region. In addition, design optimization could be performed with a significantly reduced computation time. In that field, a known model called the spring based model was used in [15–19]. These works concern mainly shear bolted joints and single-lap joints. Gray and McCarthy [20] developed a spring based analytical model for through-the-thickness stiffness prediction, which was able to calculate the joint behavior under a tensile load using the Ritz approximation. Although those methods are less time consuming and ensure excellent results, they are mainly dependent on commercial FE codes - except one developed in [20]. In addition, none of these works have been extended to casings or cylindrical composite structures, where pull through failure is combined with bearing failure. Bolted joints are generally stronger in bearing mode than pull through mode [21].

In this paper, a new semi-analytical model combining FE analysis on structural 1D elements and analytical formulations is developed for the preliminary design of a bolted joint 3D woven composite-metal casing. First, a new formulation of the orthotropic axisymmetric shell element stiffness matrix is developed. Then, a global modeling of the joint is proposed. The simplified model is applied to a relevant bolted joint of casing used in aircraft engines and the results are compared to those of 3D Finite Element Analysis. Finally, a parametric study is conducted in order to analyze the effects of geometrical and material parameters on joint behavior and asses the ability

of the developed model to predict physical behavior of the joint and its usability as a preliminary design tool.

2. Stiffness calculation in bolted joint analysis: Theoretical background

The stiffness of bolted joints is a key parameter in determining the deformation of assemblies subjected to bolt preload and external load. During the assembly of bolted joints, the bolts are in tension and clamped parts are in compression. The amount of these deformations depends on the stiffness of each assembled element and the global behavior of the assembly depends on the joint stiffness, K_{joint} , which, in turn, depends on the bolt and member stiffnesses. As shown in Figure .1b, the mechanical linear model of a pretensioned bolted joint assembly (given in Figure .1a) is schematized as linear springs of the clamped parts disposed in series and in parallel with the bolt linear spring. K_{p1} is the axial stiffness of the first part, K_{p2} is the axial stiffness of the second part and K_b is the axial stiffness of the bolt. K_{p1} , K_{p2} and K_b can be calculated as function of geometric parameters of the assembly and materials parameters of bolt and assembled parts, further details of their calculation methodology are given in sections 2.1 and 2.2. Theoretically, joint stiffness can be calculated as given in Eq.1.

Bolts allow two or many parts/flanges to be assembled by means of the pretension phase. However, bolted joints are usually subjected to external loads, such as axial load, shear load and moment, after pretension. In fact, the axial stiffness of the bolt remains unchanged, but the axial stiffness of the clamped parts depends on the loading and it has been proved that it is different from the stiffness given for the bolt load case (after preload). He et al. [22] have provided a new analytical formulation that considers this

phenomenon and have validated the methodology according to FEA results. In the case of the bolted joints studied in these works, the axial stiffness of the clamped parts is not calculated analytically at the external load step since the stiffness of clamped parts is given by the stiffness matrix of the 1D finite element model of the flange. Further details are given in Section 3.1.

$$K_{joint} = K_b + \frac{K_{p1}K_{p2}}{K_{p1} + K_{p2}} \quad (1)$$

2.1. Axial stiffness of the bolt

In most bolt modeling aimed at identifying axial bolt stiffness, the bolt is assimilated to two cylinders. The upper one represents the unthreaded part of the bolt with cross-section A_0 , including bolt head contribution, while the second one represents the threaded part with cross-section A_s , including the nut contribution. Equivalent axial stiffness K_{beq} is consequently calculated as mentioned in Eq.2, where l_0 is the unthreaded length, l_s is the threaded length, d is nominal diameter of the bolt and d_s is its resistive diameter, E_b is Young's Modulus of the bolt material, and α_t and α_e are two coefficients that represent the bolt head and nut stiffness contributions, respectively, to the bolt axial stiffness. Identification of those coefficients has been the subject of many previous studies: VDI [23] recommends using 0.4 for both coefficients. Later studies performed by Vadean et al. [24] suggest setting $\alpha_e=1.1$, whereas Fukuoka et al. [25] recommend a coefficient $\alpha_e=0.85$ obtained from finite element model computations. However, all the work mentioned above was performed for standard fasteners and consequently, they cannot be used automatically in the framework of this paper, since the bolts studied here are specific and used solely in aerospace engine structures. It was necessary to

determine coefficients α_t and α_e in adequation with the geometry of the bolts. A 3D FE analysis based on the identification of strain energy (bolt, bolt head and nut) as in [26] allowed α_t and α_e to be determined: $\alpha_t = 0.37$ and $\alpha_e = 0.4$.

$$\frac{1}{K_{beq}} = \frac{1}{E_b} \left(\frac{\alpha_t d}{A_0} + \frac{l_0}{A_0} + \frac{\alpha_e d}{A_s} + \frac{l_s}{A_s} \right) \quad (2)$$

2.2. Axial stiffness of clamped parts

At the preload step, pretension of the bolt forms a stress zone within the clamped parts which could be equivalent to two truncated pressure cones in bolted joints analysis. The other region, with zero stress, has no effect on axial stiffness of the clamped part (see Figure .1a). Identifying this stiffness comes down to determining the axial stiffness of the truncated cone. Basically, the axial stiffness of the clamped parts is determined by means of Eq.3, where K_{pi} is the axial stiffness of a subassembly, A_{pi} denotes its cross-section and L_{pi} refers to the subassembly length. The most difficult parameter to identify here is the equivalent cross section. One of the first works in that field was performed by Rasmussen et al. in [27] and suggested a formulation of the cone equivalent cross section based on Finite Elements Analysis and applied to cylindrical subassemblies. Later , Alkatan et al. [26] improved on Rasmussen's formulation and extended it to prismatic assemblies. With a mathematical approach applied to cylindrical assembled parts, VDI [23] suggested a formula for the determination of the axial stiffness of the clamped parts including the cone angle ϕ (see Figure .1a). The formulation was later demonstrated by Gornet et al. [28], based on an energetic approach. The cone angle had been introduced earlier by Rotscher [29] who fixed it at 45° . VDI [23] proposed accurate formula for angle determination according to whether the assembly was made up with bolts or fasteners. On the other

hand, Nassar and Abboud [30] proposed a new formulation for the stiffness of an assembly and its members, based on a supposed polynomial distribution of stress under the bolt head in a multimaterial joint, fixing the cone angle at 36° .

Since the application in this work concerns flange assemblies, assembled parts in the bolt region (pressure cone area) are identified neither as cylindrical parts nor as rectangular ones, so none of the methodologies mentioned above can be used directly. Thus, a complementary geometric method is proposed here. It suggests dividing an angular portion of the surface into successive elements, and associating a radius r_i with each element so that the global section of the element can be assimilated to an elementary cylinder of diameter $D_{pi} = 2 * r_i$ (see Figure .3). Then, Rasmussen's method [27] can be applied to each element to obtain A_{pi} , the equivalent cross section of the corresponding portion. Finally the equivalent global surface area of the angular portion is obtained by summing all the elementary surfaces as in Eq.4.

The methodology proposed in this paper to determine the axial stiffness of the bolt does not depend on the subassembly material since the material parameter will be introduced in equation Eq.3. The axial stiffness of isotropic materials can be easily investigated by setting E_{pi} equal to Young's modulus, but the issue is less trivial when the assembled parts are made with composite material, especially the 3D woven composite treated in this work. In a preliminary design approach, behavior of 3D woven composite is assumed to be orthotropic since the preliminary design is performed at the macroscopic scale. The question that arises is: under an orthotropic behavior

assumption, which Young's modulus should be considered for axial stiffness determination

in the case of assembled parts using 3D woven composite?. For homogenized laminates, Nelson et al. [31] suggest replacing E_{pi} by $E_L E_T$, where E_L is the longitudinal modulus and E_T the transversal one. This approach was also adopted by Gray and McCarthy in [20] but was applied to laminate composites and for thin plates ($L = 5.2mm$ and $4.16mm$) which is not the same case as studied in this paper. Thus, basic finite element computations allowed E_{pi} to be fixed at $E_{out-of-plane}$ for the thick, clamped 3D woven composite used in this work where $L = 9mm$. That seems to be justified from a physical standpoint since the main advantage of 3D woven composites is their high strength in the out-of-plane direction.

$$K_{pi} = \frac{A_{pi} E_{pi}}{L_{pi}} \quad (3)$$

$$A_p = \sum_{i=1}^n \frac{A_{pi} \phi_i}{2\pi} \quad (4)$$

3. Model development

3.1. Basics of modeling

The semi-analytical model developed here is a finite elements method based meta-model where each part of assembly is modeled with basic structural elements (2D shell elements and 1D beam elements) as shown in Figure .4. It is called a semi-analytical model because some terms of stiffness matrix of elements will be identified analytically.

Assembled flanges can be orthotropic or isotropic, so either metallic or composite materials can be considered. Bolt/flange or flange/flange interactions are modeled with DOF coupling of meshing nodes.

Contact between the assembled parts is ensured with spring elements modeling normal contact stiffness. Here, the tangential contact behavior is neglected because, under eccentric axial loading, the two parts tend to separate from each other, friction effects occur only after quasi-complete separation and are located near the ab/a^0b^0 area, and preliminary design criteria are generally reached at this step of loading. A detailed description of elements types and couplings is given below:

- $[ace]$ and $[a^0c^0e^0]$: *Axisymmetric shell elements (flange pad and shroud)*

Casings are almost geometrically symmetric and can be subjected to non-uniform loading in real life. In a preliminary design approach, most of the critical load is assumed to be applied all around the circumference so the casings can be modeled with axisymmetric shell elements. The choice to adopt axisymmetric shell theory is justified in this work since the ratio t/r_{min} is very small for the flanges studied here. The difference between $[ac]$ and $[ce]$ is on the shell orientation, 90° for $[ac]$ and 0° for $[ce]$ (see Figure .5) and, consequently, on the stiffness matrix formulation.

- $[bd]$ and $[b^0d^0]$: *Hybrid axisymmetric shell element* This element is added in order to integrate the axial stiffness of the clamped region at the preload step. Practically, axial terms of the axisymmetric shell stiffness matrix referring to axial stiffness are modified and replaced by the axial stiffness calculated in Section 2.2.

- *[xy] : Beam element*

In bolted joints subjected to eccentric axial loading, bolts are especially subject to tensile and bending stresses. An equivalent cross section, A_b , and length, l_b , can be calculated analytically as shown in Section 2.1, and Guillot [32] suggests a formulation for the equivalent moment of inertia I_b . Hence, the bolt is modeled with a beam element using Euler Bernoulli theory since the $L/d > 5$ ratio condition is verified for bolts used in the framework of this study.

- *[d⁰y]: 1D beam connector*

The beam connector allows a relation to be written between the nut and the lower flange while applying a pretension load, High Young's modulus $E_{C-beam}=10^3 E_{bolt}$, and the same cross section and moment of inertia as the bolt are assigned to this element.

Kinematic couplings are established in order to represent the physical behavior of the assembly. In general, kinematic couplings are expressed by means of linear equations defining kinematic relationships between degrees of freedom of the coupled nodes.

- *Kinematic coupling N° 1 [dx]:*

One of the hypotheses of the meta-model is that the bolt head is constrained to follow flange pad kinematics in the axial direction (displacement v), the radial direction (displacement u) and the bending direction (rotation w). This is ensured through the hybrid shell element $[bd]$. Consequently, the three DOFs at nodes d and x are constrained by a system of three equations described by the system of Eq.5, where u_i , v_i and w_i denote axial displacement, radial displacement and rotation of

node i , respectively, and Δz and Δr stand respectively for relative distance in axial and radial displacement, respectively between coupled nodes.

$$\begin{aligned} u_d &= u_x + \Delta z * w_x \\ v_d &= v_x - \Delta r * w_x \\ w_d &= w_x \end{aligned} \tag{5}$$

- *Kinematic coupling N° 2 [d⁰y]:*

When pretension is applied to the bolt, a relative axial displacement is created. This displacement is allowed by setting a sliding link between nodes y^0 and d^0 . Consequently, the preload can be applied at nodes y and y^0 .

$$\begin{aligned} u_{y^0} + u_{d^0} &= 0 \\ w_{y^0} + w_{d^0} &= 0 \end{aligned} \tag{6}$$

- *Kinematic coupling N° 3 [aa⁰]:*

The purpose here is to prevent any sliding of flange pad so that tangential contact stiffness can be neglected. Radial displacements of nodes a and a^0 which are assumed to remain in contact during loading, are coupled. The equation Eq.7 describes this coupling.

$$v_a + v_{a^0} = 0 \tag{7}$$

3.2. Orthotropic shell element stiffness

Identification of the axisymmetric shell stiffness matrix for isotropic materials has been the subject of many studies. However, they fewer for

orthotropic materials. Thus, an attempt is made in this work to identify the stiffness matrix of an orthotropic shell element based on the Direct Stiffness Method proposed by Turner [33] and used by Rockey [34], who identified the axisymmetric shell element stiffness of isotropic materials. This methodology is adapted to orthotropic materials by expressing the stress resultants and taking orthotropic behavior into account according to Eq.8, where N and M are membrane and bending stress resultants, and χ refer to membrane or curvature deformation, t is the shell thickness, E denotes Young's modulus and ν is Poisson's ratio. L and T stand for the longitudinal and transversal directions (equivalent to the *weft* and *warp* directions shown in Figure .6).

$$\begin{bmatrix} N_L \\ N_T \\ M_L \\ M_T \end{bmatrix} = \frac{t}{1 - \nu_{LT}\nu_{TL}} \begin{bmatrix} E_L & E_L\nu_{TL} & 0 & 0 \\ E_T\nu_{LT} & E_T & 0 & 0 \\ 0 & 0 & \frac{t^2}{12}E_L & \frac{t^2}{12}E_L\nu_{TL} \\ 0 & 0 & \frac{t^2}{12}E_T\nu_{LT} & \frac{t^2}{12}E_T \end{bmatrix} \begin{bmatrix} \epsilon_L \\ \epsilon_T \\ \chi_L \\ \chi_T \end{bmatrix} \quad (8)$$

3.3. Bolt stiffness

The bolt is modeled with a beam element with equivalent cross-section A_{beq} , length l_{beq} and moment of inertia I_{beq} calculated as shown in eqs. (9) to (11) by integrating both threaded and unthreaded parts. The Classical stiffness matrix of an Euler Bernoulli beam element is used.

$$A_{beq} = \frac{l_0 + l_s}{\frac{l_0 + \alpha_e d}{A_0} + \frac{l_s + \alpha_t d}{A_s}} \quad (9)$$

$$l_{beq} = l_0 + \alpha_e d + l_s + \alpha_t d \quad (10)$$

$$I_{beq} = \frac{l_0 + l_s}{\frac{l_0}{I_0} + \frac{l_s}{I_s}} \quad (11)$$

3.4. Contact stiffness

Contact between pad flanges is modeled with linear spring elements. The axial stiffness of each spring is identified according to Chakhari et al. [35] who suggest suggested that the stress distribution of contact stiffness is proportional to theoretical contact area (see Figure .7), so the axial stiffness K_{ci} can be calculated as it is related to the total contact stiffness K_c by Eq.12. L_i and L_{i-1} are the sizes of the two shell elements adjacent to the linear spring i and L_c denotes the total contact length.

Total contact stiffness is taken to be proportional to joint stiffness by using an adjusting parameter, C_{rep} , given by Eq.13, convergence allowed this parameter to be set to $C_{rep} = 0.19$.

$$K_i = K_c * 0.5 * \frac{L_{i-1} + L_i}{L_c} \quad (12)$$

$$K_c = \frac{K_{joint}}{C_{rep}} \quad (13)$$

3.5. Resolution

A simplified scheme for the resolution of the model algorithm developed is shown in Figure .8. The first step is to define meshing parameters and identify the element stiffness matrix based on data for geometry and materials.

Then, kinematic couplings are set between the nodes involved. The global stiffness matrix, K_g , describing the problem is established by assembling the

stiffnesses of all elements of the assembly which were initially established in their local coordinate systems and are transferred to the global coordinate system (r,z,θ) , and by including mathematical formulations of kinematic couplings. As a first loading, the bolt preload, F_0 , is installed in the beam element modeling the bolt. Hence, loads F_0 and $-F_0$ are applied at nodes y and y^0 respectively. An initial system of linear equations given by Eq.14 is resolved. U is the vector of node displacement, K_g is the global matrix stiffness including the stiffness of all springs, and F stands for the load vector. Here, all contact springs stiffnesses contribute to the global contact stiffness, so an iterative resolution is necessary in order to identify and include only compressed springs in the global stiffness matrix while removing stiffnesses of spring elements that are subjected to tensile loading. This approach was adopted by Chakhari in [35]. Converged computation is reached when two successive resolutions give the same compressed springs.

Then, preload results are transferred to the external loading step, as the relative bolt displacement $v_{r_{preload}}$ due to the preload is expressed as an additional kinematic coupling given by Eq.15, which fixes the bolt length due to preload. Integration of this coupling is carried out according to methodology used for other kinematic couplings. A new global stiffness is consequently calculated together with load vector $[F]$ including external load F_{ext} applied at node e . The same resolution procedure as used at the preload step is followed for each load increment.

$$[U] = [K_g]^{-1}[F] \quad (14)$$

$$v_x + v_y = v_{r_{preload}} \quad (15)$$

4. Finite Element Analysis

4.1. FE Analysis of axisymmetric orthotropic flanges

An axisymmetric finite element model using 2D elements as shown in Figure .9 was established in Abaqus software in order to validate the stiffness matrix of orthotropic shell elements modeling the flange.

The flange is constrained at the right end of the pad and a pressure is applied at the left end section of the shrouded flange with an equivalent axial load $F_e = 250 \text{ kN}$. 4-node bilinear axisymmetric quadrilateral elements CAX4 are used and 4 elements are set along the flange thickness. Orthotropic elastic behavior is chosen by introducing engineering constants given in Table .1. No damage behavior of the composite flange is considered since the purpose is to assess an adapted definition of the orthotropic shell linear stiffness matrix proposed in this work.

4.2. 3D FE Analysis of bolted flanges connection

In order to assess the semi-analytical model of a multi-material bolted joint integrating 3D woven composite structures, a Python-Abaqus routine is developed for the automated creation of an equivalent 3D FE model in Abaqus software according to the geometry and materials used in the semianalytical model. The case studied here is based on a real bolted joint of casings with approximate dimensions (Figure .11). It is an angular portion of 1.33° with one bolt. Eight-node solid linear brick incompatible elements are used (C3D8I) are used in order to better capture the bending behavior and 6 elements are set along flange thickness. These elements are commonly used in this type of applications. Axial, radial and rotational displacements of the right end section of the metallic flange are constrained at zero during all steps

of the simulation. At the preload step boundary conditions (that will be called $BC_{preload}$ as indicated in Figure .10) are set in order to eliminate rigid body motion, accelerate computation and allow displacement of the bolt in the axial direction only.

A preload $F_0 = 20 \text{ kN}$ is applied at section [AB] with the Bolt Preload function included in Abaqus. Parameters of the composite flange materials are the same as given in Table .1 and isotropic behavior is assigned to the metallic flange, with $E = 210000 \text{ GPa}$ and $\nu = 0.3$.

Contact behavior with a very small friction coefficient is defined for bolt head/composite flange, composite flange/metallic flange and metallic flange/nut contacts. Frictionless behavior cannot be defined because of numerical convergence problems that may potentially occur. Finally, an increasing external axial load from $F_e = 0$ to 10 kN with an increment of 0.5 kN is applied at the left end section of the composite flange and $BC_{preload}$ boundary conditions are deactivated.

5. Results and discussion

5.1. Orthotropic axisymmetric shell element validation

A comparison was made between the numerical formulation of orthotropic shell elements based on Rockey's [34] method extended to orthotropic materials and the 2D axisymmetric FE computation performed in Abaqus software. Figure .12 shows a visualization of the deformed configuration under maximum load ($F_e = 250 \text{ kN}$). Because of the considerable length of the shrouded flange, a large deflection is observed at

the end of flange corner in both simulations; the global behavior is qualitatively the same.

Displacement of the flange at the section where the load is applied (node for semi-analytical model) was investigated. Figure .14 shows LoadDisplacement curves for both axial and radial displacement. The results are in good agreement with the axisymmetric 2D FE model particularly for radial displacement. The semi-analytical model is more accurate in predicting radial displacement than axial displacement. This can be explained by the fact that shear effects are not taken into account in the semi-analytical model. This effect is especially marked at the pad part because of the low t/L ratio. Consequently, a correcting factor of $C_s = 0.75$ was proposed in order to avoid this shortcoming and was applied to the stiffness matrix of the 90° axisymmetric shell (pad part). Figure .15 shows Load-Displacement curves after correction: the axial displacement is now more accurate and this correction does not affect radial displacement results.

The accuracy of the semi-analytical model was also observed to depend on the element length chosen for shell elements, especially at the pad part. A parametric study of meshing size at this area (see Figure .13) allowed the element size to be set at 3 mm for the given application and showed that it is advisable to avoid using small element size $< 1\text{ mm}$, as numerical lock occurs with small thick elements.

Hence, the formulation developed for orthotropic axisymmetric shell elements is validated and semi-analytical results are in good agreement with the axisymmetric FE calculations using 2D elements. This formulation can be used for a semi-analytical model of flanges of composite-metal bolted joints.

5.2. Semi-analytical model validation

An equivalent semi-analytical model of the 3D FE model shown in Figure .11 was developed. Shell elements were positioned at the middle of the flange thickness. In order to validate the semi-analytical model, a comparison was made with the preliminary design criteria identified earlier for this type of bolted joints: bolt normal stress σ_{Nbolt} that results in tensile stress of the bolt σ_{tbolt} and bending stress of the bolt σ_{fbolt} , equivalent axial load P and bending moment M at cross-section S_{fl} (cf. Figure.16), axial displacement $v_{aflange}$ and at node N highlighted in .16b).

In the 3D FE model, displacements are obtained directly when the tensile and bending stresses of the bolt are calculated as given in Eq.16, where σ_A and σ_B are the axial stresses at node A and B respectively (see Figure .10). The flange shroud and pad are meshed according to the mesh size parametric study results found earlier e.g. 11 mm for shroud shell elements and 3 mm at the pad part.

$$\begin{aligned}\sigma_{tbolt} &= \frac{\sigma_A + \sigma_B}{2} \\ \sigma_{fbolt} &= \frac{\sigma_A - \sigma_B}{2} \\ \sigma_{Nbolt} &= \sigma_{tbolt} + \sigma_{fbolt}\end{aligned}\tag{16}$$

The global behavior of the assembly was similar for the two simulations. Figure .17 shows the assembly state obtained with semi-analytical and 3D FE models at the final axial loading increment. At the preload step, flanges are under compression and the bolt is subjected to a tensile stress. Axial displacement of the orthotropic flange is in the opposite direction and higher than for the metallic flange since the latter is stiffer in the out-of-plane direction. After the preload, increasing of the axial load leads to a progressive

separation of the two flanges. At $F_e = 4 \text{ kN}$, separation takes place near the bolt and the external load creates a tensile stress higher than preload on the bolt, thus leading to a bending moment creating strong bending stress.

5.2.1. Bolt behavior

As explained above, an axial load applied to the composite flange leads to a tensile and bending stress in the bolt. These stresses were investigated by comparing results given by the semi-analytical and 3D FE models. Variations of tensile stress, bending stress and consequently normal stress are plotted versus external load in Figure .18. Before $F_e = 4 \text{ kN}$, the bolt is subjected mainly to its preload, with a small amount of bending stress. After separation, the slope becomes greater and bending stress increases. This is typical of bolt behavior in eccentric axial bolted joints. The results show very good agreement between the semi-analytical model and the 3D FE computation. The gap observed at the beginning of the simulation is due to the preload state transfer (displacement of the bolt) to the loading step. The maximum absolute error observed is 17 MPa for tensile stress and 15 MPa for bending stress. The maximum relative error for normal stress, taking the 3D FE computation as a reference, was 1,6%.

5.2.2. Flange behavior

The deformed shape of the assembly shows a good prediction of flange behavior under an external eccentric axial load. In order to quantify the simulation results, the variation of the mean moment and axial load seen by section S_{fl} under external loading is plotted in Figure .19a and .19b respectively. The results show very good agreement between the semi-analytical model and FE model computation for effort and moment. The gap observed for the Mean Moment is also due to the preload state transfer and

is about 9%. At preload, the composite flange undergoes slight bending caused by the hybrid element stiffness. However, it can be observed that the semi-analytical model underestimates axial displacement of the composite flange when compared to the 3D finite element model. Since efforts and moments are well represented, this means that the issue is located near the bolt: local behavior near the bolt inhibits the joint displacement and this can be related to the formulation of the hybrid element. It seems that this element's stiffness is overestimated and makes the assembly stiffer. This issue will be treated in future works since the present state of the model reproduces the global assembly behavior and is able to predict design criteria in a preliminary design approach.

5.2.3. *Contact behavior*

Contact status between the two flanges changes with axial loading. Among the design criteria related to contact behavior that are usually verified for eccentric axial we find the separation load. This load is characterized by the load for which the contact area goes beyond the bolt hole. Basically, it corresponds to the load for which the curve of tensile stress-vs load for the bolt changes slope, which means at $F_e = 4 \text{ kN}$. In order to assess the robustness of the semi-analytical model in predicting contact behavior, a comparison is established between contact status evolution during loading given by the semi-analytical model and that found with the 3D FE model. Analyses are based on separation location and contact area. Within the semi-analytical model, contact area is identified by the total length of compressed springs, schematized when the upper flange (in red) penetrates the lower one (in blue) (see Figure .20). At the preload step, a separation occurs near

the shroud due to the eccentricity of the load, it is confirmed that this phenomenon is well reproduced by the semi-analytical model. However, a very slight bending of the assembly is observed due to the presence of the hybrid element which bridges the gap observed for the mean moment at S_{fl} at the beginning of the loading step. During loading, the contact area moves to the right end of the pad flanges with a decrease of contact area. Figure .20 shows the contact status at the preload step, at the separation point and by the end of the simulation. The semi-analytical model is able to predict the load at separation well and to quantify the contact area.

6. Parametric study

A parametric study was run on the semi-analytical model of a bolted joint of two flanges, where the metallic flange was fixed. Various material parameters were set for the composite flange, in the aim of proving the ability of the developed model to provide the physical responses of flange assemblies and to demonstrate its usability in running parametric studies for preliminary design goals within a strongly reduced computation time. The assembly geometry considered here is similar to the one studied for model validation with $\alpha = 0^\circ$ and $\alpha^0 = 0^\circ$. The test combinations performed in the developed model are summarized in Table .2.

6.1. Effect of preload

Properly preloaded bolted joints ensure an efficient design and allow a variety of problems to be overcome, such as fatigue failure, joint separation, and self-loosening through vibration. Thus, the study of the preload effect is

necessary to define the optimum preload level in a bolted joint. The results of tests 1, 2 and 3 concerning normal stress and axial displacement of the joints are plotted in Figure.21. A low preload leads to a rapid joint separation and affects the axial displacement of the loaded flange, which increases after separation.

6.2. Effect of bolt position

Among the design parameters that a designer has to set are the bolt position in flanged assemblies: its eccentricity reveals the joint behavior of the joints. The results of tests 2, 4 and 5 are plotted in Figure .22. The slope after separation increases with increase in the radius of the bolt position radius. Highly eccentric loading leads to a fast joint separation and creates an initial bending effect at the beginning of loading. Consequently, the earlier the separation occurs, the higher is the axial flange displacement as there is no contact stiffness to maintain the joint. The location of the bolt hole near the corner can avoid early separation of flanges but it should be coherent with geometrical constraints and ensure enough space for tightening.

6.3. Effect of material properties

Increasing of the longitudinal modulus of a composite flange has practically no effect on bolt behavior before separation. After separation, the effect of E_L mostly concerns the shroud behavior. A low Young's modulus in that direction logically leads to a high axial displacement and, consequently, a little additional stress on the bolt. These observations are consistent with results obtained from tests 2, 6 and 7 (see Figure .23).

7. Conclusion

This work has dealt with the development and validation of a new semianalytical model for 3D woven composite-metallic bolted joints of flanges assemblies based on a direct stiffness method that consists of FE computation using 1D structural elements. A formulation of the stiffness matrix of orthotropic shell elements has been proposed and validated with respect to a 2D FE axisymmetric model. Based on this formulation, a semi-analytical model of a multi-material eccentric axial bolted joint was developed. Stress on the bolt, flange behavior and contact status given by the model developed were compared to a 3D FE model. Results are in very good agreement and relative error does not exceed 9% for bending moment of the flange and 2% for normal stress on the bolt. this model divided the computation time by a factor of about gain 120 in comparison with a 3D FE model. However, results for axial displacements were less accurate. Work is currently in progress to solve this issue by considering a new stiffness matrix for the hybrid element. Finally, a parametric study on different model parameters shows the ability of the simplified model to ensure physical responses, thus proving its usability for running optimization studies and its reliability as a preliminary design tool.

Acknowledgements

The collaboration with Safran Aircraft Engines is gratefully acknowledged. This work was supported under PRC MECACOMP, French research project co-funded by DGAC and Safran Group, piloted by Safran Group and involving Safran Group, Clément Ader Institute and CNRS.

Data availability

The raw/processed data required to reproduce these findings cannot be shared at this time due to legal or ethical reasons.

References

- [1] A. E. Bogdanovich, Multi-scale modeling, stress and failure analyses of 3-d woven composites, *Journal of Materials Science* 41 (2006) 6547–6590. doi:10.1007/s10853-006-0197-2.
- [2] A. P. Mouritz, M. K. Bannister, P. Falzon, K. Leong, Review of applications for advanced three-dimensional fibre textile composites, *Composites Part A: Applied Science and Manufacturing* 30 (1999) 1445–1461. doi:10.1016/S1359-835X(99)00034-2.
- [3] B. Cox, M. Dadkhah, R. Inman, W. Morris, J. Zupon, Mechanisms of compressive failure in 3d composites, *Acta Metallurgica et Materialia* 40 (1992) 3285–3298. doi:10.1016/0956-7151(92)90042-D.
- [4] K. C. Warren, R. A. Lopez-Anido, J. Goering, Behavior of threedimensional woven carbon composites in single-bolt bearing, *Composite Structures* 127 (2015) 175–184. doi:10.1016/j.compstruct.2015.03. 022.
- [5] M. McCarthy, V. Lawlor, W. Stanley, C. McCarthy, Bolt-hole clearance effects and strength criteria in single-bolt, single-lap, composite bolted joints, *Composites Science and Technology* 62 (2002) 1415–1431. doi:10. 1016/S0266-3538(02)00088-X.

- [6] V. P. Lawlor, M. A. McCarthy, W. Stanley, An experimental study of bolt-hole clearance effects in double-lap, multi-bolt composite joints, *Composite Structures* 71 (2005) 176–190. doi:10.1016/j.compstruct.2004.09.025.
- [7] D. Elder, A. Verdaasdonk, R. Thomson, Fastener pull-through in a carbon fibre epoxy composite joint, *Composite Structures* 86 (2008) 291–298. doi:10.1016/j.compstruct.2008.03.041.
- [8] L. Adam, C. Bouvet, B. Castanié, A. Daidié, E. Bonhomme, Discrete ply model of circular pull-through test of fasteners in laminates, *Composite Structures* 94 (2012) 3082–3091. doi:10.1016/j.compstruct.2012.05.008.
- [9] K. C. Warren, R. A. Lopez-Anido, S. S. Vel, H. H. Bayraktar, Progressive failure analysis of three-dimensional woven carbon composites in single-bolt, double-shear bearing, *Composites Part B: Engineering* 84 (2016) 266–276. doi:10.1016/j.compositesb.2015.08.082.
- [10] P. P. Camanho, F. Matthews, A progressive damage model for mechanically fastened joints in composite laminates, *Journal of Composite Materials* 33 (1999) 2248–2280. doi:10.1177/002199839903302402.
- [11] M. McCarthy, C. McCarthy, V. Lawlor, W. Stanley, Three-dimensional finite element analysis of single-bolt, single-lap composite bolted joints: Part I model development and validation, *Composite Structures* 71 (2005) 140–158. doi:10.1016/j.compstruct.2004.09.024.

- [12] C. McCarthy, M. McCarthy, W. Stanley, V. Lawlor, Experiences with modeling friction in composite bolted joints, *Journal of Composite Materials* 39 (2005) 1881–1908. doi:10.1177/0021998305051805.
- [13] J. Ekh, J. Schön, Finite element modeling and optimization of load transfer in multi-fastener joints using structural elements, *Composite Structures* 82 (2008) 245–256. doi:10.1016/j.compstruct.2007.01.005.
- [14] P. Gray, C. McCarthy, A highly efficient user-defined finite element for load distribution analysis of large-scale bolted composite structures, *Composites Science and Technology* 71 (2011) 1517–1527. doi:10.1016/j.compscitech.2011.06.011.
- [15] W. Barrois, Stresses and displacements due to load transfer by fasteners in structural assemblies, *Engineering Fracture Mechanics* 10 (1978) 115–176. doi:10.1016/0013-7944(78)90055-3.
- [16] C. McCarthy, P. Gray, An analytical model for the prediction of load distribution in highly torqued multi-bolt composite joints, *Composite Structures* 93 (2011) 287–298. doi:10.1016/j.compstruct.2010.09.017.
- [17] M. McCarthy, C. McCarthy, G. Padhi, A simple method for determining the effects of bolt–hole clearance on load distribution in singlecolumn multi-bolt composite joints, *Composite Structures* 73 (2006) 78–87. doi:10.1016/j.compstruct.2005.01.028.
- [18] M. McCarthy, J. Xiao, C. McCarthy, A. Kamoulakos, J. Ramos, J. Gallard, V. Melito, Modelling bird impacts on an aircraft wing–part 2: Modelling the

- impact with an sph bird model, *International Journal of Crashworthiness* 10 (2005) 51–59. doi:10.1533/ijcr.2005.0325.
- [19] A. Olmedo, C. Santiuste, E. Barbero, An analytical model for the secondary bending prediction in single-lap composite bolted-joints, *Composite Structures* 111 (2014) 354–361. doi:10.1016/j.compstruct.2014.01.015.
- [20] P. Gray, C. McCarthy, An analytical model for the prediction of throughthickness stiffness in tension-loaded composite bolted joints, *Composite Structures* 94 (2012) 2450–2459. doi:10.1016/j.compstruct.2012.02.011.
- [21] A. Banbury, D. Kelly, A study of fastener pull-through failure of composite laminates. part 1: Experimental, *Composite Structures* 45 (1999) 241–254. doi:10.1016/S0263-8223(99)00009-4.
- [22] P. He, J. Liu, C. Zhang, Z. Liu, Analytical modeling of axial stiffness of tensile bolted joints under concentric external load, *Journal of Mechanical Science and Technology* 33 (2019) 5285–5295. doi:10.1007/s12206-019-1020-8.
- [23] Systematische Berechnung hochbeanspruchter Schraubenverbindungen: Mehrschraubenverbindungen : Blatt 2. Systematic calculation of highly stressed bolted joints. multi bolted joints : part 2, VDI, Berlin, 2014. URL: <https://cds.cern.ch/record/1987643>.

- [24] A. Vadean, D. Leray, J. Guillot, Bolted joints for very large bearing numerical model development, *Finite Elements in Analysis and Design* 42 (2006) 298–313. doi:10.1016/j.finel.2005.08.001.
- [25] T. Fukuoka, T. Takaki, Elastic plastic finite element analysis of bolted joint during tightening process, *Journal of Mechanical Design* 125 (2003) 823–830. doi:10.1115/1.1631579.
- [26] F. Alkatan, P. Stephan, A. Daidie, J. Guillot, Equivalent axial stiffness of various components in bolted joints subjected to axial loading, *Finite Elements in Analysis and Design* 43 (2007) 589–598.
- [27] J. Rasmussen, I. Norgaard, O. Haastrup, Haastrup, A two body contact problem with friction, in: *Euromech Colloquium NR*, volume 110, 1978, pp. 115–120.
- [28] L. Gornet, R. Hamonou, F. Jacquemin, S. Auger, Compliance determination of a bolt structure with the help of a homogenization approach: application for composite materials, in: *Proceedings of Journ´ee Nationale des Composites (JNC20)*, 2017.
- [29] F. Rotscher, *Die maschinenelemente*, Springer-Verlag 234 (1927).
- [30] S. A. Nassar, A. Abboud, An improved stiffness model for bolted joints, *Journal of Mechanical Design* 131 (2009) 121001. doi:10.1115/1.4000212.
- [31] W. D. Nelson, B. L. Bunin, L. J. Hart-Smith, *Critical Joints in Large Composite Aircraft Structure.*, Technical Report, MCDONNELL DOUGLAS CORP LONG BEACH CA DOUGLAS AIRCRAFT DIV, 1983.

- [32] J. GUILLOT, Assemblages par ´el´ements filet´es. calcul, Techniques de l’ing´enieur. G´enie m´ecanique (1987) B5560–1.
- [33] M. J. Turner, R. W. Clough, H. C. Martin, L. Topp, Stiffness and deflection analysis of complex structures, journal of the Aeronautical Sciences 23 (1956) 805–823.
- [34] K. C. Rockey, H. Evans, D. Griffiths, D. A. Nethercot, The finite element method - a basic introduction, Strain 11 (1975) 140–140.
- [35] J. Chakhari, A. Daidi´e, Z. Chaib, J. Guillot, Numerical model for twobolted joints subjected to compressive loading, Finite Elements in Analysis and Design 44 (2008) 162–173. doi:10.1016/j.finel.2007.11.010.
- [36] S. Yan, X. Zeng, A. Long, Meso-scale modelling of 3d woven composite t-joints with weave variations, Composites Science and Technology 171 (2019) 171–179. doi:10.1016/j.compscitech.2018.12.024.

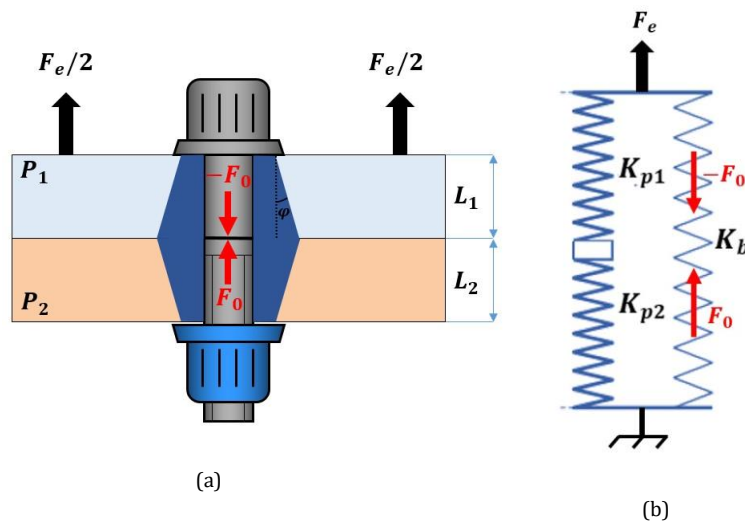


Figure .1. Simplified illustration of pretensioned bolted joint with an equivalent crosssection under tensile load (a) and equivalent joint stiffness model (b).

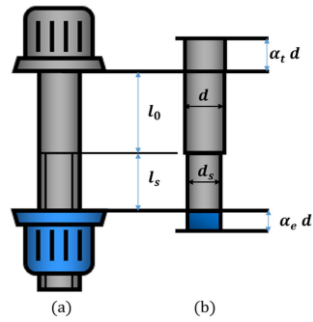


Figure .2. Real bolt (a) and simplified bolt model (b).

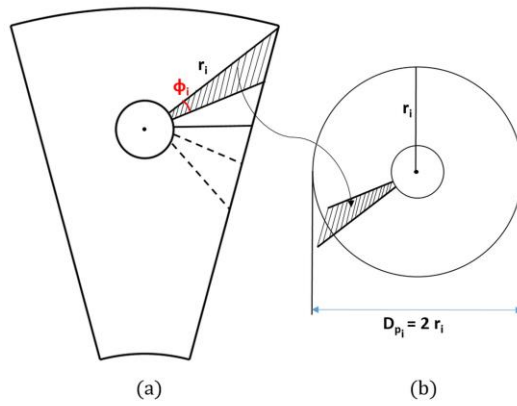


Figure .3. Principle of geometrical adaptation of angular portion of clamped parts flange assemblies for axial stiffness calculation: angular portion (a) and equivalent circular portion (b).

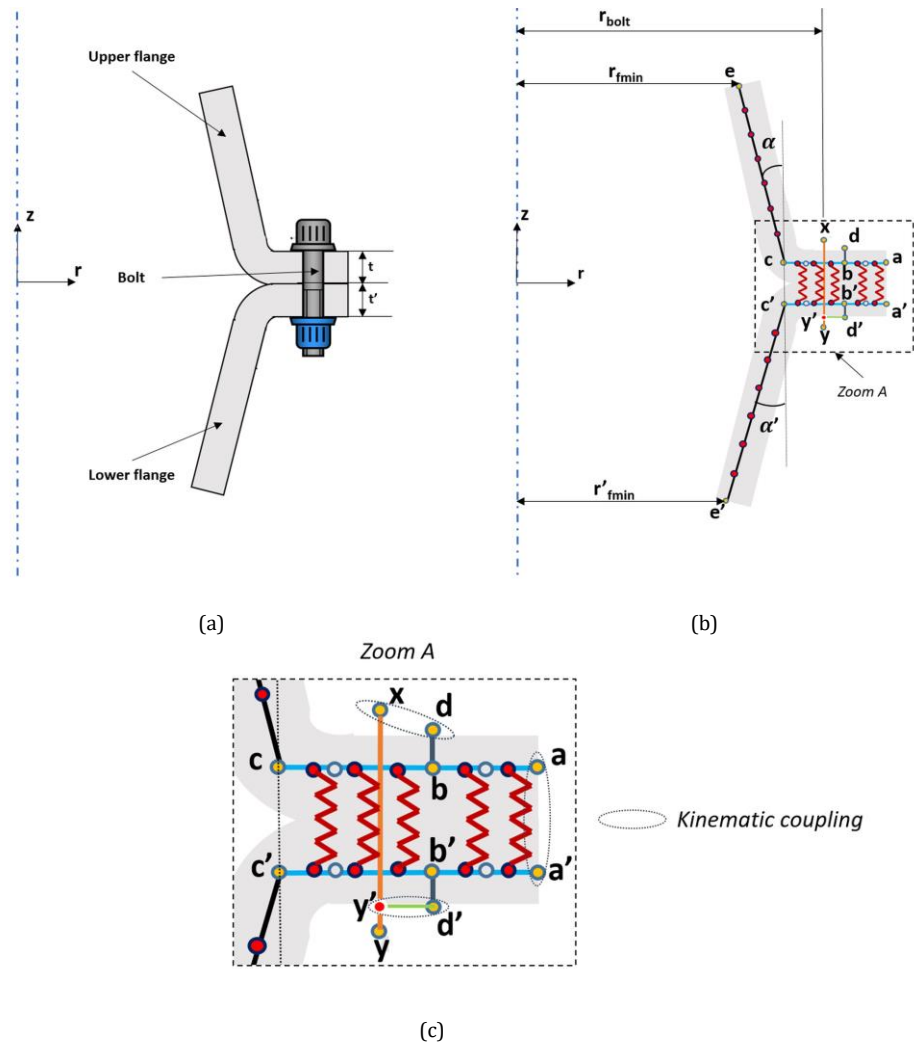


Figure .4. Simplified scheme of bolted flanges assembly (a) and semi-analytical modelling principles (b) with a zoom on the contact area (c).

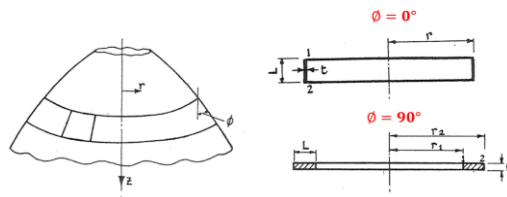


Figure .5. Geometrical shell definition and orientation (Rockey [34]).

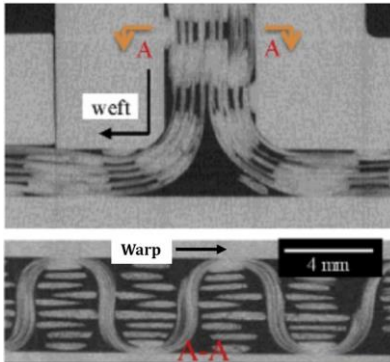


Figure .6. Images from μCT scan of a 3D woven composite flange provided by Yan et al. in [36] with a highlight on warp and weft directions.

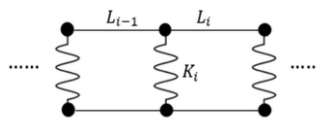


Figure .7. Principle of linear spring element axial stiffness calculation.

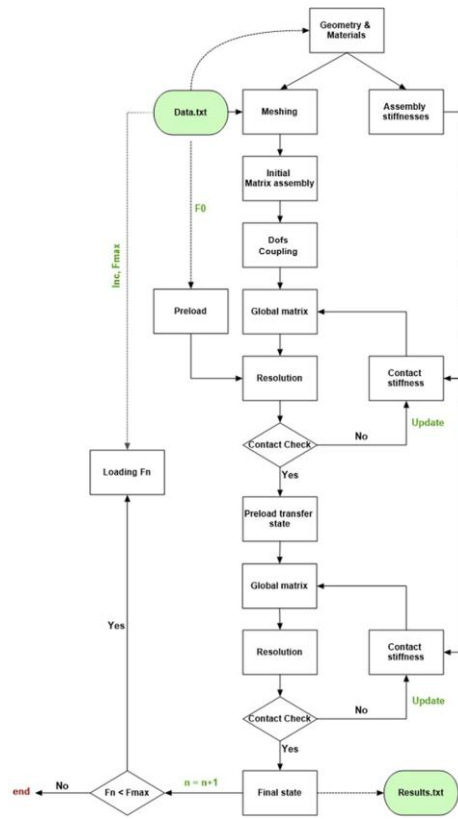


Figure .8. Algorithm resolution of the semi-analytical model.

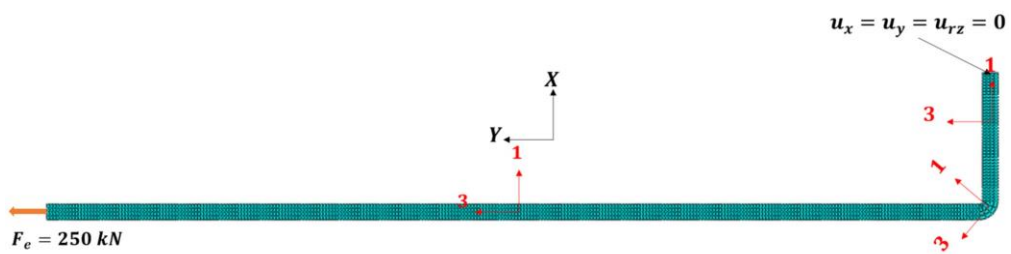


Figure .9. Axisymmetric FE model of the flange using 2D elements and subjected to axial loading.

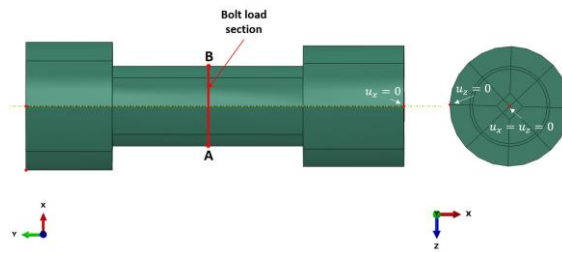


Figure .10. Boundary conditions $BC_{preload}$ defined on the bolt at the preload step.

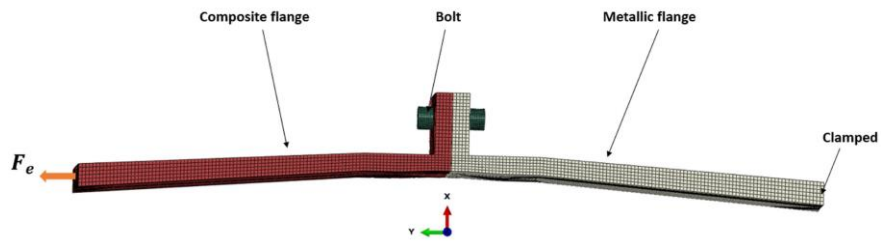


Figure .11. 3D FE model of the flanges bolted joint case study

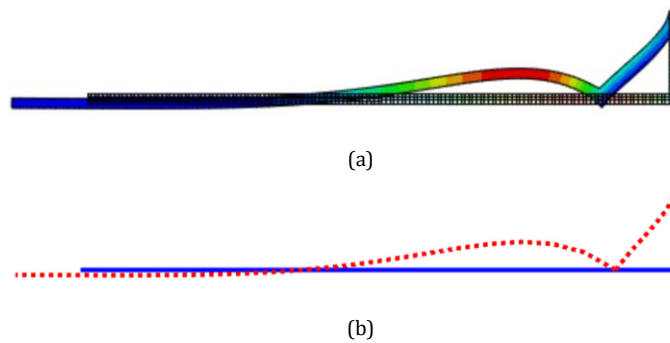


Figure .12. Deformed shape with x50 amplification of the orthotropic flange given with the 2D axisymmetric FE model (a) and with the semi-analytical model (b).

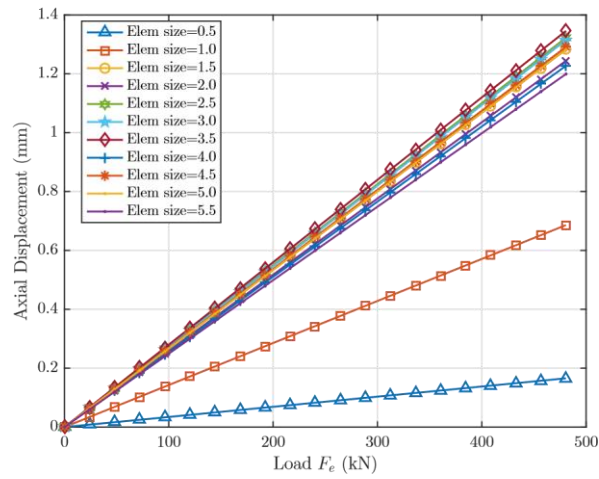


Figure .13. Influence of elements' mesh size at the pad part on axial flange displacement given by the semi-analytical model.

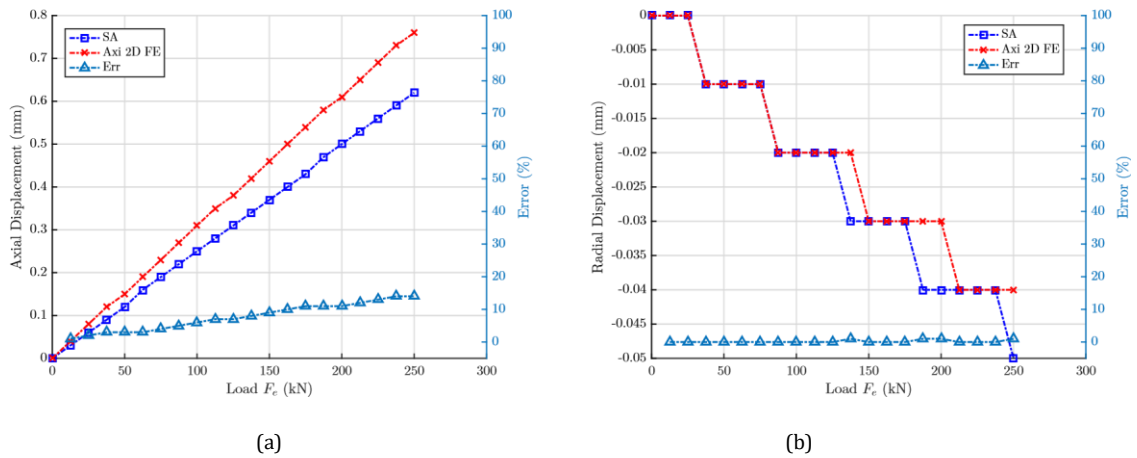
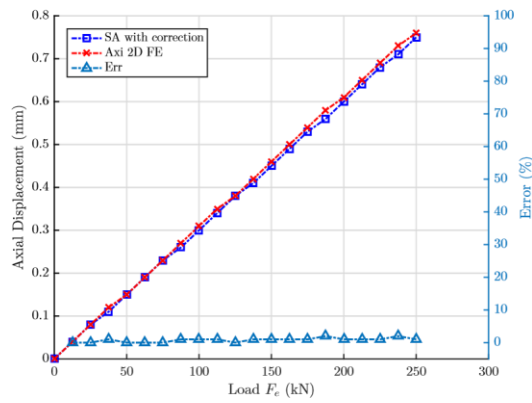
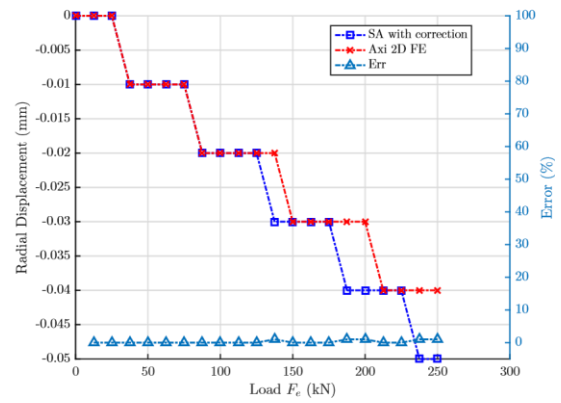


Figure .14. Comparison of axial displacement (a) and radial displacement (b) at left end section between semi-analytical model and axisymmetric FE model.

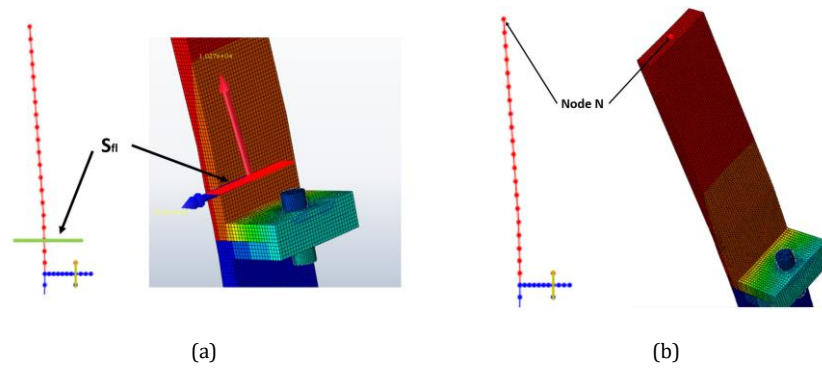


(a)



(b)

Figure .15. Comparison of axial displacement (a) and radial displacement (b) at section S between semi-analytical model and 2D axisymmetric FE model after setting correcting factor $C_s = 0.75$.



(a)

(b)

Figure .16. Section where flange bending moment and axial load are retrieved (a) and calculation principle of tensile and bending stress of the bolt (b).

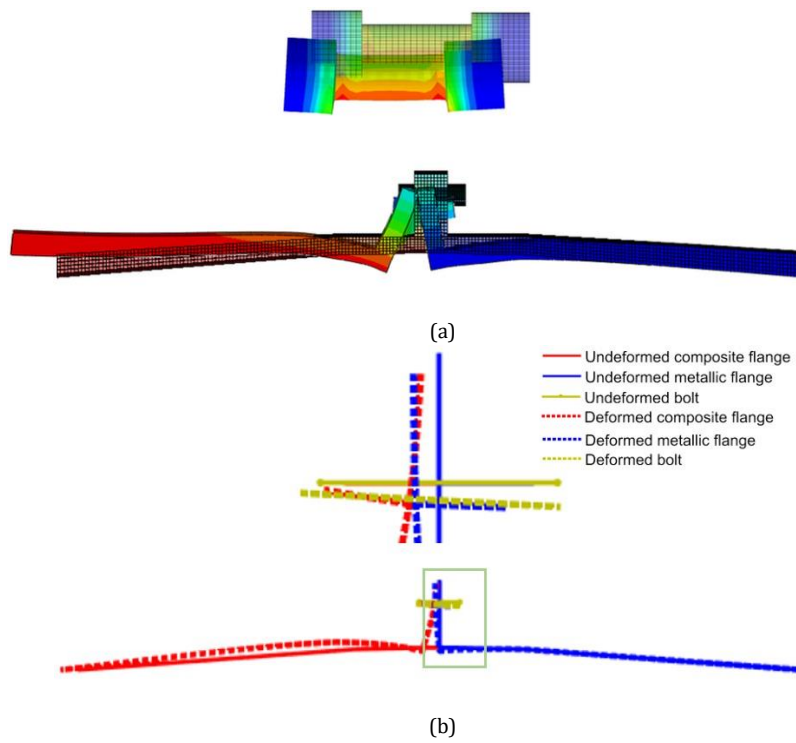
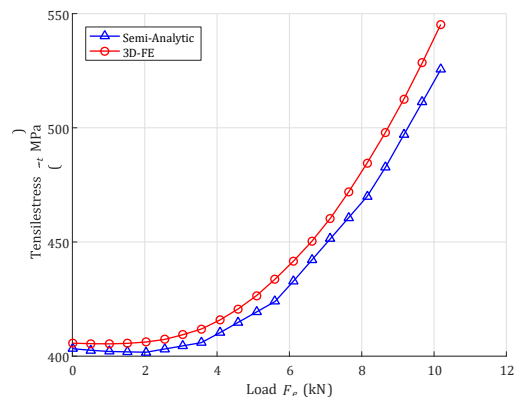
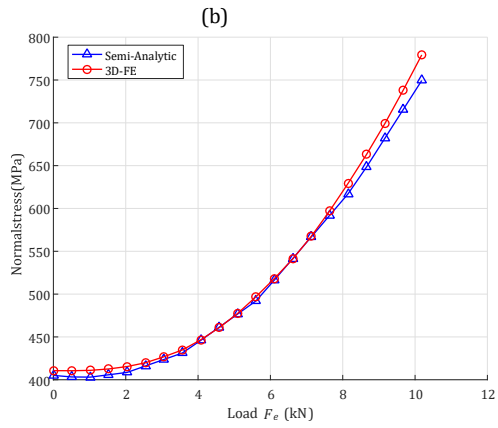
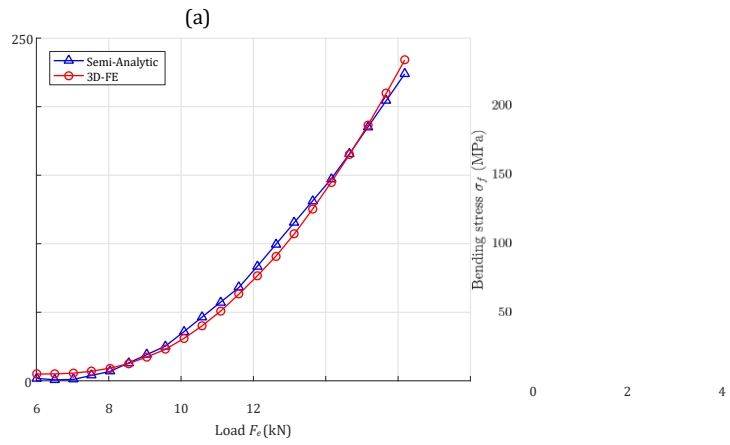


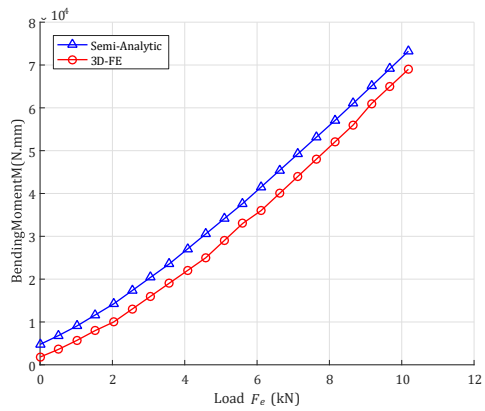
Figure .17. Global behavior of the Composite-Metallic bolted joints given with 3D FE model (a) and semi-analytical model (b).



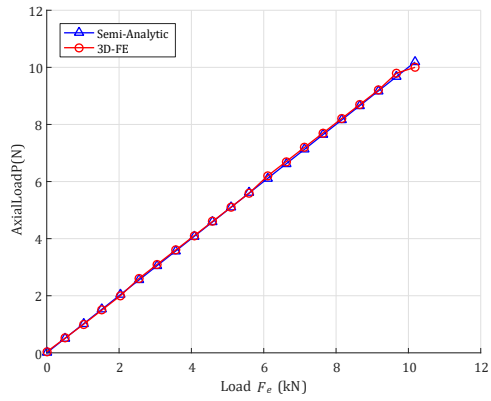


(c)

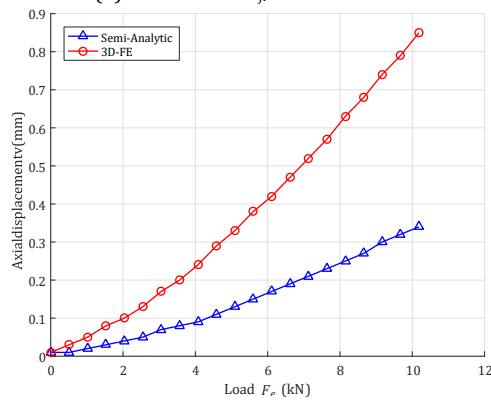
Figure .18. Comparison between 3D FE model and semi-analytical model, for tensile stress (a), bending stress (b) and normal stress (c) criterion at the section [AB] of the bolt.



(a) Bending Moment at S_f section



(b) Axial load at S_{η} section



(c) Axial displacement at node N

Figure .19. Comparison of composite flange behavior between 3D FE model and semianalytical model.

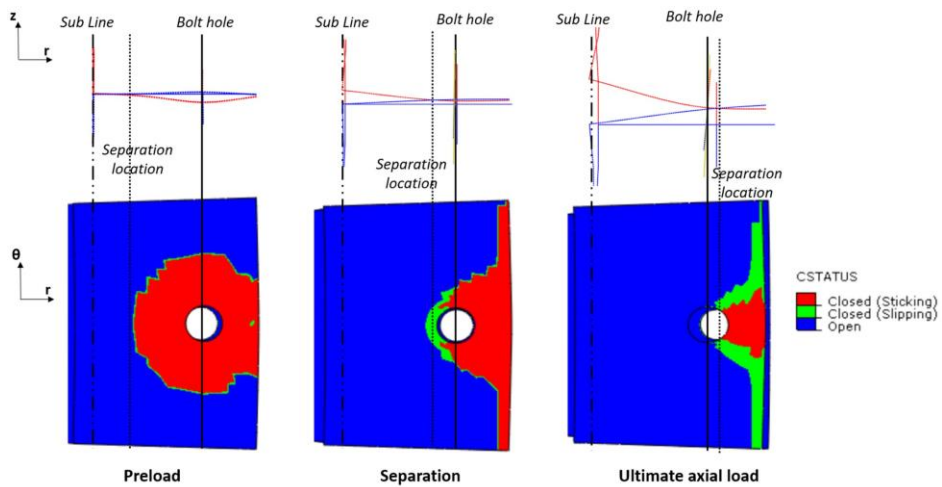


Figure .20. Comparison of contact status between 3D FE model and semi-analytical model.

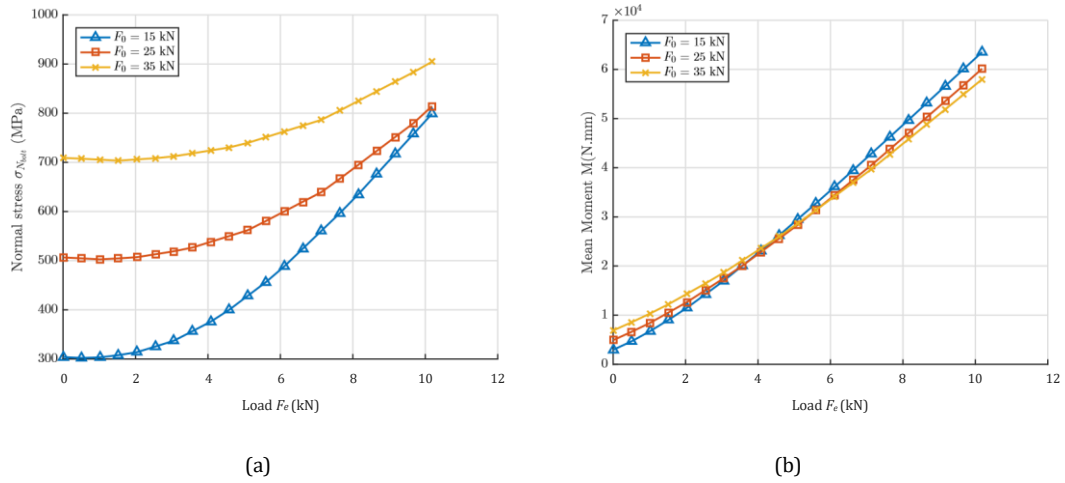


Figure .21. Effect of preload on normal stress of the bolt (a) and on axial displacement of the composite flange (b).

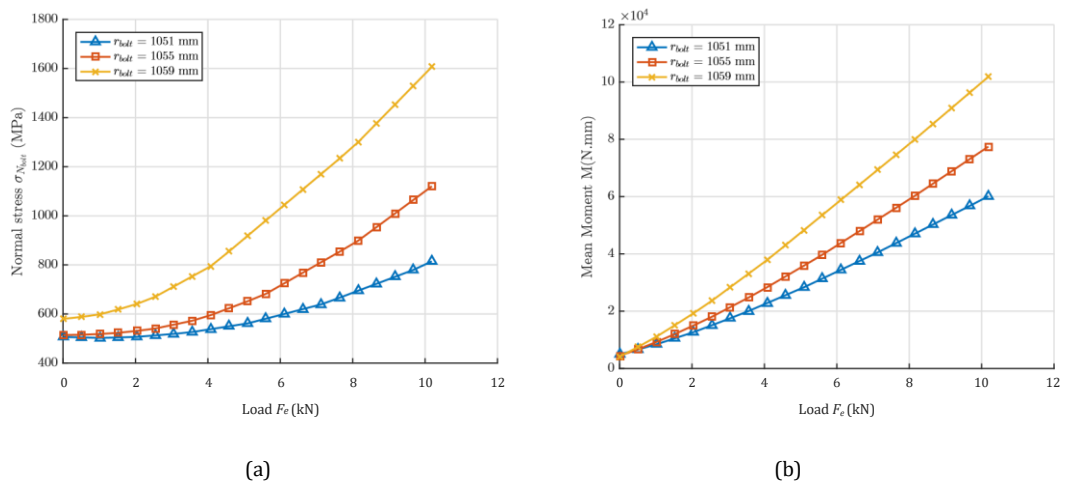


Figure .22. Effect of bolt position on normal stress of the bolt (a) and on axial displacement of the composite flange (b).

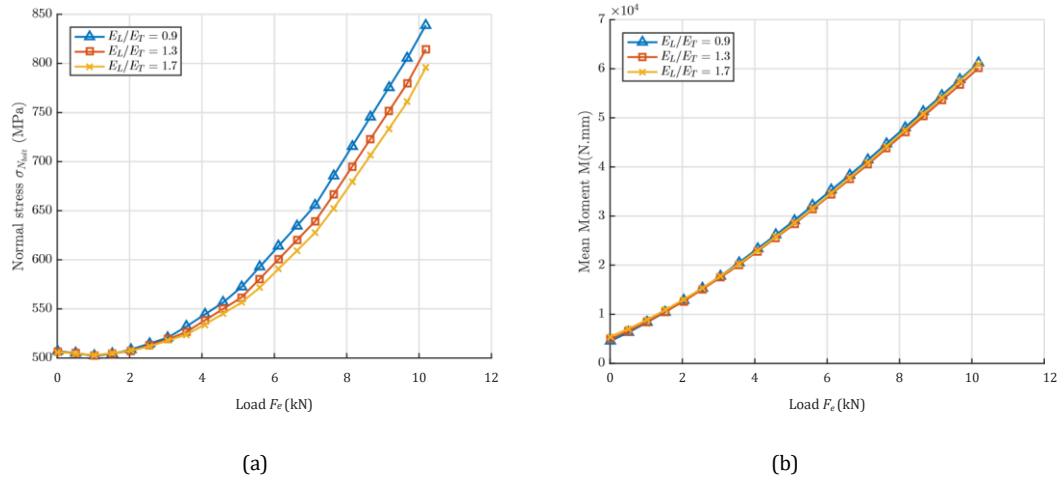


Figure .23. Effect of composite material parameters on normal stress of the bolt (a) and on axial displacement of the composite flange (b).

Table .1. Material properties of flange.

E_1/E_2	E_1/E_3	ν_{12}/ν_{13}	ν_{12}/ν_{23}	G_{12}/G_{13}	G_{12}/G_{23}
1.3	8.6	0.04	0.05	1.4	1.3

Table .2. Parametric study test matrix.

Test N°	F_0 (kN)	r_{bolt} (mm)	E_L/E_T
1	15	1051	1.3
2	25	1051	1.3
3	35	1051	1.3
4	25	1055	1.3
5	25	1059	1.3
6	25	1051	0.9
7	25	1051	1.6